Enhanced Atlantic sea level rise relative to the Pacific under high carbon emission rates

J. P. Krasting[1], J. P. Dunne[1], R. J. Stouffer[1], and & R. W. Hallberg[1]

[1]*NOAA/Geophysical Fluid Dynamics Laboratory, Princeton, New Jersey, USA*

Thermal expansion of the ocean in response to warming is an important component of historical sea level rise[1]. Observational studies show that the Atlantic and Southern oceans are warming faster than the Pacific Ocean[2–5]. Here we present simulations using a numerical atmospheric-ocean general circulation model with an interactive carbon cycle to evaluate the impact of carbon emission rates, ranging from 2 to 25 GtC yr^{-1}, on basin-scale ocean heat uptake and sea level. For a given level of cumulative emissions, sea level rise is largest at low emission rates, confirming the variable proportionality between cumulative emissions and sea level rise[6]. For simulations with emission rates greater than 5 GtC yr^{-1}, sea level rise is larger in the Atlantic than Pacific Ocean on centennial timescales. In these transient scenarios, basin-scale asymmetry is related to the shorter Atlantic flushing timescales and weakening of the overturning circulation. We conclude that Atlantic coastal areas may be particularly vulnerable to sea level rise from present-day high greenhouse gas emission rates, while low future emission rates of 2 and 3 GtC yr^{-1} will cause relatively larger sea level rise in the Pacific on millennial timescales.

Recent observational efforts [3,4] have improved the understanding of heat and carbon uptake especially above the thermocline. The oceans have also taken up nearly a quarter of the carbon

emissions related to fossil-fuel burning and land use changes[7], while more than 90% of the anthropogenically-generated heat anomaly between 1971 and 2010 has gone into warming the oceans[8]. These studies have demonstrated the Atlantic basin is warming faster than the Pacific[2–5]. Among other factors, variability-enhanced heat uptake in both the Atlantic[9] and Pacific[10] has thought to have played a role in the recent "hiatus decade" in global warming (2000-2009)[10]. We show here the carbon emission rate also forces basin scale differences in oceanic heat and carbon uptake as well as SLR on longer timescales (i.e. centennial and millennial).

To examine the role of emission rate on basin area-average differences in SLR, we use a series of idealized climate change scenarios[11] where a fully coupled climate-carbon-cycle model, GFDL-ESM2G, is forced with a range of seven different carbon emission rates: 2, 3, 5, 10, 15, 20, and 25 GtC yr^{-1}. Following a 1,000 year spin-up of the model, a 1,200 year control run was performed with preindustrial forcing. Three ensemble members of each experiment were integrated for 200 years (400 years in the 5GtC/yr case and 1,200 years in the 2 and 3 GtC/yr cases) in order to achieve at least a doubling of atmospheric CO_2. The centennial-scale effects of model drift were also removed from the experiments (see methods).

The role of ventilation timescale on the rate of warming in the individual ocean basins is a key determinant making the Atlantic basin area-average SLR greater than the Pacific in transient climate scenarios. We use ocean ideal age[12] (see methods) to assess the ventilation timescales of the individual basins. In GFDL-ESM2G, the average age of the Atlantic basin at the beginning of the preindustrial control run is 225 years while the average age of the Pacific is 600 years.

Although the total volume of the Pacific Basin is approximately double that of the Atlantic, the factor of 3 difference between their ages illustrates the Atlantic has a larger volume of recently ventilated water than the Pacific (Supplementary Fig. S1). The Atlantic basin convective overturning introduces younger waters into the basin through North Atlantic Deep Water (NADW) and Antarctic Bottom Water (AABW). A shallow overturning circulation also exists in the North Pacific, but the primary source of deep water is via the Southern Ocean.

As the surface ocean warms in response to carbon emissions, the upper ocean becomes increasingly stratified over time and reduces the rate of deep water formation[13]. After 200 years (Fig. 1), high carbon emission rates (i.e. 25 GtC yr^{-1}) result in a 12 Sv ($\sim$50%) reduction in the strength of the Atlantic Meridional Overturning Circulation (AMOC), where 1 Sv $\equiv 10^6$ m^3 s^{-1}. Lower carbon emission rates, (i.e. 2 and 5 GtC yr^{-1}) also result in a weaker AMOC (3 and 6 Sv, respectively), but the change is not as large as in the high emission rate case.

Weaker overturning cells in the Atlantic make the ocean interior both warmer and less ventilated through reductions in NADW and AABW formation. Under high emission rates (25 GtC yr^{-1}), the change in the basin-average age after 200 years normalized by its initial age (ΔA_N) is approximately a factor of 3 larger in the Atlantic than in the Pacific (Supplementary Fig. S2). This ratio of the age anomaly between the Atlantic and Pacific basins is approximately the same as the inverse ratio of their average ideal ages from the control run (226 years / 598 years = 0.38). In the lower emission rate cases after 200 years, the Atlantic to Pacific ratio of ΔA_N is at or below 1 (2 GtC $yr^{-1} \approx 0.5$; 2 GtC $yr^{-1} \approx 1$) indicating a more uniform aging of the two basins.

The Atlantic minus Pacific temperature changes as a function of depth (Fig. 2) illustrate the role of emission rate in enhancing the inter-basin differences. Since upper ocean temperatures (0-700m) are well-correlated with sea surface temperatures on decadal timescales, the largest temperature changes occur in the upper ocean under high emission rates. The Atlantic warms faster than the Pacific in the upper ocean and the difference between the two basins are similar for a given cumulative emissions level ($\Delta T \approx 0.4C$ at 2000 GtC) regardless of the emission rate (Fig. 2a, dots). Thus, the inter-basin differences in SLR depend on how much the rest of the water column experiences the warming signal. While SLR is not proportional to cumulative emissions[6], cumulative emissions are a potential predictor of the upper ocean temperature differences between the Atlantic and Pacific basins above the thermocline.

At very low carbon emission rates (2 and 3 GtC yr^{-1}), deep ocean (2000-5500m) temperature differences between the Atlantic and Pacific peak after several centuries then decrease. The initial increase in deep Atlantic warming relative to the Pacific reflects the faster turnover rates in the Atlantic. As the simulations approach the ventilation timescales of the Pacific (basin-average ideal age of 600 years, Supplementary Fig. S1), the Atlantic and Pacific continue to warm at similar rates. Additionally, as atmospheric CO_2 concentrations increase, they become less effective at increasing the radiative forcing[14]. In the very low emissions case, this produces a response where the climate is in quasi-equilibrium with the atmospheric CO_2 concentration. Relative to the beginning of the simulation, each turnover cycle introduces less heat into the Atlantic and more into the Pacific, thus reducing the inter-basin differences on millennial timescales.

Temperature and carbon differences between the two basins are similar when averaging across the entire depth of the ocean (0 to 5500m), and both are dominated by their mid and upper ocean contributions (0 to 2000m) on the timescales considered here. However, their behavior in the deep ocean (Fig. 2c,g) illustrates key differences between them. Temperature changes are a reflection of both additional warming as well associated circulation changes. Carbon, however, behaves more like a passive tracer. The long-term accumulation of both heat and carbon in the deep ocean will likely differ between the two basins on millennial timescales. This has possible implications for the combination heat and carbon uptake to continue to act as a stabilizing mechanism for the Transient Climate Response to cumulative carbon Emissions (TCRE) on these timescales[15].

The inter-basin differences in heat uptake associated with varying emission rates are reflected in the model's representation of SLR (see methods). Both the Atlantic and Pacific basins experience SLR (Fig. 3) but the amount of SLR in the Atlantic is greater than the Pacific at emission rates >5 GtC yr^{-1}, where it exceeds the range of variability from the preindustrial control run. As the simulations approach the timescales of ventilation in the Pacific basin (600 years) in the very low emission rate (2 and 3 GtC yr^{-1}) scenarios, basin area-average SLR in the Pacific becomes larger than the Atlantic. The Pacific overtakes Atlantic sea level, as the mean depth of the Pacific is deeper than the Atlantic (as shown in Supplementary Fig. S3) and there is a deeper average column to warm. In the limit of quasi-equilibrium with the climate forcing, the Atlantic-to-Pacific SLR difference would likely converge among the emission rate scenarios as the timescales of adjustment are independent of the magnitude of the forcing[16]

With respect to time in these experiments, the higher carbon emission rates produce the largest SLR (Fig. 3a-c). With respect to cumulative emissions, however, the lower emission rates produce the largest SLR at a given cumulative emissions amount (Fig. 3e-g). For a given level of cumulative carbon emissions, the longer timescales associated with low emission rates allow a larger volume of the ocean to undergo warming. The ensemble mean ratio of Atlantic to Pacific area-average SLR plotted against cumulative emissions peaks at values near 3 (after initial variability), which is similar to the ratio of the changes in volume mean age between the basins discussed earlier. The Atlantic to Pacific SLR ratio decreases in all runs towards the ratio from the control run (0.83) as the oceans attempt to reach quasi-equilibrium with the climate forcing.

To further illustrate the relationship between carbon emission rate, duration of emissions, and the differences between the Atlantic and Pacific basin, we plot the difference patterns of SLR averaged over years 61-100 for the 2, 5, and 25 GtC yr^{-1} scenarios relative to the control run (Fig. 4a-c). The largest SLR occurs in the Atlantic in all three cases, but the differences are more clear in the high emission rate case for normalized emergent patterns of SLR (see methods) particularly along the US east coast and the southern tip of Greenland (Fig. 4d-f). The inter-basin differences are more evident when comparing the scenarios at 2000 GtC of cumulative carbon emissions. The normalized patterns of SLR are most uniform between the basins in the 2 GtC yr^{-1} case while SLR is almost exclusively seen in the Atlantic in the 25 GtC yr^{-1} case.

As with all state-of-the-art earth system models, careful interpretation of GFDL-ESM2G must note important caveats. The GOLD ocean model component used in GFDL-ESM2G has local

biases (as much as 0.5m) in dynamic sea level based on comparisons of CORE-II-forced simulations with AVISO altimetry observations (1993-2007)[17] but are similar in magnitude to those found in other models[17]. While the current study has focused on the basin area-average SLR, it is important to note other factors that have significant contributions to SLR in the real world. These include geoid changes, glacial isostatic adjustment, as well as freshwater mass contributions from melting land ice which have implications for the strength of AMOC[18].

The patterns of enhanced Atlantic SLR in the idealized GFDL-ESM2G simulations shown in this study agree well with the CMIP5 ensemble mean response to the RCP scenarios [19,20], since the RCP scenarios are mainly driven by CO_2 increases. Furthermore, enhanced Atlantic SLR occurs following a shutdown of the thermohaline circulation in previous generation models[21]. The details of our results may vary depending on the individual model representation of AMOC and the associated age distributions among the world's ocean basins. The results may also depend on ocean mixing and the equilibrium climate sensitivity, which vary from model to model. It is worth noting that variations in heat uptake efficiency and thermal expansion efficiency across models [22], could also impact these results. Although individual models may vary based on all of these factors, the results of this study are potentially reproducible in the CMIP5 multi-model ensemble, mainly since the ventilation timescales of the Atlantic are shorter than the Pacific (Supplementary Fig. S1).

Local effects[1,23] such as land subsidence, changes in offshore winds, and ocean circulation changes (i.e. AMOC) lead to sea levels that are rising faster than the global average along the U.S.

East Coast. Our results suggest that higher carbon emission rates also contribute to increased SLR in this region compared to the global average. The basin area-average differences in SLR between the low and high carbon emission rate cases are relevant to climate adaptation efforts because they illustrate the relative vulnerability of the Atlantic to high emission rates and demonstrate that global average metrics of SLR could become less representative of regional scale changes.

Methods

The GFDL-ESM2G model used in this study is a fully coupled Atmosphere-Ocean General Circulation Model (AOGCM) with an interactive carbon cycle. The model was developed by NOAA's Geophysical Fluid Dynamics Laboratory and participated in the Fifth Coupled Model Intercomparison Project[24] (CMIP5). GFDL-ESM2G uses approximately a 2° spatial resolution for the atmosphere and land components and a 1° spatial resolution for the ocean component. The model uses the same atmospheric component (AM2) used in the GFDL-CM2.1 model[25]. In the configuration used for this study, atmospheric CO_2 concentrations are predicted directly by the coupled model. The land component of GFDL-ESM2G, LM3, includes a dynamic vegetation component[26]. Potential vegetation is used in these experiments (i.e. no land use) and the model produces an above ground preindustrial global biomass of ∼850 GtC. LM3 does not include the effects of nitrogen limitation on vegetation growth. The Generalized Ocean Layer Dynamics (GOLD) model[27] is used to simulate the physical ocean. GOLD uses a 63-layer isopycnal coordinate interior which reduces numerical diapycnal mixing and permits more physically based mixing parameterizations. A spatially dependent geothermal heat flux, which averages ∼0.1

W/m^2 globally, was applied at the ocean floor. The Tracers Of Phytoplankton and Allometric Zooplankton (TOPAZ) model[27] is coupled to the GOLD ocean to simulate ocean carbon dynamics - including biogeochemistry and primitive ecology. Model source code is available at http://www.gfdl.noaa.gov/earth-system-model.

Compared with the RAPID array observing system[28] at 26.5N, the simulation of AMOC by GFDL-ESM2G is stronger than the observations (23.6 $\pm$ 1.7 Sv vs. 18.5 $\pm$ 4.9 Sv), while the poleward heat transport is consistent with the observations (1.14 PW vs. 1.33 $\pm$ 0.40 PW). A full description of the models and their validation are presented in two papers by Dunne et al. (2012)[27,29].

The idealized carbon emission rate scenarios apply a persistent carbon flux to the model's lowest atmospheric layer evenly over the non-glacial land points in the model. This carbon flux is the only forcing applied to the model. In this experimental design[11], all other model forcing (i.e. other well-mixed GHGs, aerosols, solar) is held constant at the values used in the CMIP5 preindustrial control simulation of the model. The range of emission rates in this study (2 to 25 GtC yr^{-1}) is similar to the range of carbon emission rates at year 2100 across all of the Representative Concentration Pathways (RCPs)[30] used in the Fifth Assessment Report of the Intergovernmental Panel on Climate Change (IPCC AR5). For reference, emissions from fossil fuel combustion and cement production averaged 8.3 $\pm$ 0.7 GtC over the decade 2002-2011[7]. Each scenario was run long enough to achieve a doubling of preindustrial atmospheric CO2, with a minimum simulation length of 200 years in order to explore the multidecadal and centennial scale response to forcing.

We use the ocean ideal age tracer[12] in the model to assess the amount of ventilation in the basins. The age tracer is a passive tracer in the ocean that measures the time since a given water mass was last in contact with the surface. Lower values of the age tracer are indicative of younger more-ventilated water masses, while higher values are indicative of older and less-ventilated water masses.

Model SLR in this analysis is defined as the sum of the contributions from steric sea level changes, dynamical changes, changes in ocean mass (precipitation, evaporation, runoff, and net sea ice melt), the atmospheric inverse barometer effect, and the pressure from sea ice loading on the model's free surface. The areal extent, height, and albedo of non-interactive glaciers and ice sheets are specified in the model and their potential melt water is not considered for SLR in these experiments. Centennial scale trends in temperature, carbon, and SLR were removed by subtracting the perturbation experiments from the control run where the fields were smoothed using 100-year boxcar filter on 3-D grid point basis.

The differences of SLR shown in Figure 4 represent the initial change in sea level averaged over years 61-100 relative to the control run. A 40-year averaging period was chosen to reduce the influence of decadal scale variability (Figure 4, a-c). The "emergent patterns" were also normalized by both the global average SLR and the local, i.e. grid point, standard deviation (σ):

$$\frac{SLR_{i,j} - \overline{SLR}}{\sigma_{i,j}} \tag{1}$$

The normalization was performed to help improve the signal-to-noise ratio in the analysis, particularly for the very low (2 and 5 GtC yr^{-1}) emission rate scenarios.

The Atlantic basin was defined as all water north of the Cape of Good Hope, South Africa and includes the Arctic Ocean but does not include Hudson Bay or the Mediterranean, Baltic, or Black Seas. The Pacific basin was defined as all water north of Melbourne, Australia but does not include the Indian Ocean basin (Supplementary Fig. S3).

1. Church, J. A. *et al.* Sea level change. In Stocker, T. *et al.* (eds.) *Climate Change 2013: The Physical Science Basis. Contribution of Working Group I to the Fifth Assessment Report of the Intergovernmental Panel on Climate Change* (Cambridge University Press, Cambridge, United Kingdom and New York, NY, USA, 2013).

2. Carton, J. A. & Santorelli, A. Global decadal upper-ocean heat content as viewed in nine analyses. *J. Climate* **21**, 6015–6035 (2008).

3. Purkey, S. G. & Johnson, G. C. Warming of global abyssal and deep southern ocean waters between the 1990s and 2000s: Contributions to global heat and sea level rise budgets. *J. Climate* **23**, 6336–6351 (2010).

4. Levitus, S. *et al.* World ocean heat content and thermosteric sea level change (0–2000 m), 1955–2010. *Geophys. Res. Lett.* **39**, L10603 (2012).

5. Robson, J., Sutton, R., Lohmann, K., Smith, D. & Palmer, M. D. Causes of the rapid warming of the North Atlantic Ocean in the mid-1990s. *J. Climate* **25**, 4116–4134 (2012).

6. Solomon, S., Plattner, G.-K., Knutti, R. & Friedlingstein, P. Irreversible climate change due to carbon dioxide emissions. *Proc. Natl. Acad. Sci. U.S.A.* **106**, 1704–1709 (2009).

7. Ciais, P. *et al.* Carbon and other biogeochemical cycles. In Stocker, T. *et al.* (eds.) *Climate Change 2013: The Physical Science Basis. Contribution of Working Group I to the Fifth Assessment Report of the Intergovernmental Panel on Climate Change* (Cambridge University Press, Cambridge, United Kingdom and New York, NY, USA, 2013).

8. Rhein, M. *et al.* Observations: Ocean. In Stocker, T. *et al.* (eds.) *Climate Change 2013: The Physical Science Basis. Contribution of Working Group I to the Fifth Assessment Report of the Intergovernmental Panel on Climate Change* (Cambridge University Press, Cambridge, United Kingdom and New York, NY, USA, 2013).

9. Chen, X. & Tung, K.-K. Varying planetary heat sink led to global-warming slowdown and acceleration. *Science* **345**, 897–903 (2014).

10. Meehl, G. A., Arblaster, J. M., Fasullo, J. T., Hu, A. & Trenberth, K. E. Model-based evidence of deep-ocean heat uptake during surface-temperature hiatus periods. *Nature Clim. Change* **1**, 360–364 (2011).

11. Krasting, J. P., Dunne, J. P., Shevliakova, E. & Stouffer, R. J. Trajectory sensitivity of the transient climate response to cumulative carbon emissions. *Geophys. Res. Lett.* **41**, 2520–2527 (2014).

12. Thiele, G. & Sarmiento, J. L. Tracer dating and ocean ventilation. *J. Geophys. Res.-Oceans* **95**, 9377–9391 (1990).

13. Stouffer, R. J. & Manabe, S. Response of a coupled ocean–atmosphere model to increasing atmospheric carbon dioxide: Sensitivity to the rate of increase. *J. Climate* **12**, 2224–2237 (1999).

14. Myhre, G., Highwood, E. J., Shine, K. P. & Stordal, F. New estimates of radiative forcing due to well mixed greenhouse gases. *Geophys. Res. Lett.* **25**, 2715–2718 (1998).

15. Matthews, H. D., Gillett, N. P., Stott, P. A. & Zickfeld, K. The proportionality of global warming to cumulative carbon emissions. *Nature* **459**, 829–832 (2009).

16. Stouffer, R. J. Time scales of climate response. *J. Climate* **17**, 209–217 (2004).

17. Griffies, S. M. *et al.* An assessment of global and regional sea level for years 1993–2007 in a suite of interannual CORE-II simulations. *Ocean Model.* **78**, 35 – 89 (2014).

18. Manabe, S. & Stouffer, R. J. Simulation of abrupt climate change induced by freshwater input to the North Atlantic Ocean. *Nature* **378**, 165–167 (1995).

19. Yin, J. Century to multi-century sea level rise projections from CMIP5 models. *Geophys. Res. Lett.* **39**, L17709 (2012).

20. Bilbao, R. F., Gregory, J. & Bouttes, N. Analysis of the regional pattern of sea level change due to ocean dynamics and density change for 1993–2099 in observations and CMIP5 AOGCMs. *Clim. Dyn.* 1–20 (2015).

21. Levermann, A., Griesel, A., Hofmann, M., Montoya, M. & Rahmstorf, S. Dynamic sea level changes following changes in the thermohaline circulation. *Clim. Dyn.* **24**, 347–354 (2005).

22. Kuhlbrodt, T. & Gregory, J. M. Ocean heat uptake and its consequences for the magnitude of sea level rise and climate change. *Geophys. Res. Lett.* **39**, L18608 (2012).

23. Horton, R. *et al.* Ch. 16: Northeast. In Melillo, J. M., Richmond, T. T. & Yohe, G. W. (eds.) *Climate Change Impacts in the United States: The Third National Climate Assessment* (U.S. Global Change Research Program, 2014).

24. Taylor, K. E., Stouffer, R. J. & Meehl, G. A. An overview of CMIP5 and the experiment design. *Bull. Am. Meteorol. Soc.* **93**, 485–498 (2011).

25. Delworth, T. L. *et al.* GFDL's CM2 global coupled climate models. Part I: Formulation and simulation characteristics. *J. Climate* **19**, 643–674 (2006).

26. Shevliakova, E. *et al.* Carbon cycling under 300 years of land use change: Importance of the secondary vegetation sink. *Global Biogeochem. Cycles* **23**, GB2022 (2009).

27. Dunne, J. P. *et al.* GFDL's ESM2 global coupled climate–carbon earth system models. Part I: Physical formulation and baseline simulation characteristics. *J. Climate* **25**, 6646–6665 (2012).

28. Johns, W. E. *et al.* Continuous, array-based estimates of atlantic ocean heat transport at 26.5 °N. *J. Climate* **24**, 2429–2449 (2010).

29. Dunne, J. P. *et al.* GFDL's ESM2 global coupled climate–carbon earth system models. Part II: Carbon system formulation and baseline simulation characteristics. *J. Climate* **26**, 2247–2267 (2013).

30. Vuuren, D. *et al.* The representative concentration pathways: an overview. *Clim. Change* **109**, 5–31 (2011).

Acknowledgements We thank A. Adcroft, K. Dixon, and three anonymous reviewers for their comments and feedback on this study. We also thank C. Raphael for assistance in preparing the figures for this manuscript.

Author Contributions JPK designed the study and conducted the experiments. JPK and JPD performed the analysis of the results. All authors contributed to the interpretation of the results and assisted in writing the manuscript.

Competing Interests The authors declare that they have no competing financial interests.

Correspondence Please address all correspondence to J. P. Krasting (email: john.krasting@noaa.gov).

Figure 1 Ensemble mean Atlantic Meridional Overturning Circulation (AMOC) averaged over model years 181-200.

Units are Sv, where 1 Sv $\equiv 10^6$ m^3 s^{-1}. The average of the three ensemble members is shown for each of the idealized emission scenarios. **a**, preindustrial control run. **b**, 2 GtC yr^{-1}. **c**, 5 GtC yr^{-1}. **d**, 25 GtC yr^{-1}.

Figure 2 Atlantic minus Pacific differences in basin-average volume mean ocean temperature and dissolved inorganic carbon (DIC) concentration.

Temperature units are $^\circ$C; DIC units are mol kg^{-1}. Solid lines represent ensemble means for each emission scenario; shading represents the range among ensemble members. Dots designate when the simulations reach 200 GtC of cumulative carbon emissions. **a**, temperature change, surface to 700m. **b**, temperature change, surface to 2000m. **c**, temperature change, 2000 to 5500m. **d**, temperature change, surface to 5000m. **e-h**, same as a-d except for DIC.

Figure 3 Basin area-average differences in sea level rise (SLR) as a function of emission rate.

Units are m. Solid lines represent ensemble means for each emission scenario; shading represents the range among ensemble members. Dots indicate either 200 GtC of cumulative carbon emissions (a-d) or 200 years (e-h). **a-c**, global, Pacific, and Atlantic SLR vs. time. **d**, Atlantic minus Pacific SLR vs. time. **e-g**, same as a-c, except SLR vs. cumulative emissions. **h**, ratio of Atlantic to Pacific SLR (smoothed by a 100 GtC boxcar filter) vs. cumulative emissions. Grey dashes represent mean Atlantic to Pacific sea level (0.83) from the control simulation.

Figure 4 Spatial patterns of sea level rise (SLR) under varying emission rates.

Units are m (panels a-c) and standard deviation (σ, panels d-i). The average of the three ensemble members is shown for each emission scenario. **a-c**, SLR differences for years 61 to

100 relative to the control simulation for the 2, 5, and 25 GtC yr^{-1} scenarios. **d-f**, emergent SLR difference patterns (see methods) for the 2, 5, and 25 GtC yr^{-1} scenarios. **g-i**, normalized difference patterns in SLR (same method as panels d-f) after 2000 GtC of cumulative emissions in the 2, 5, and 25 GtC yr^{-1} scenarios.

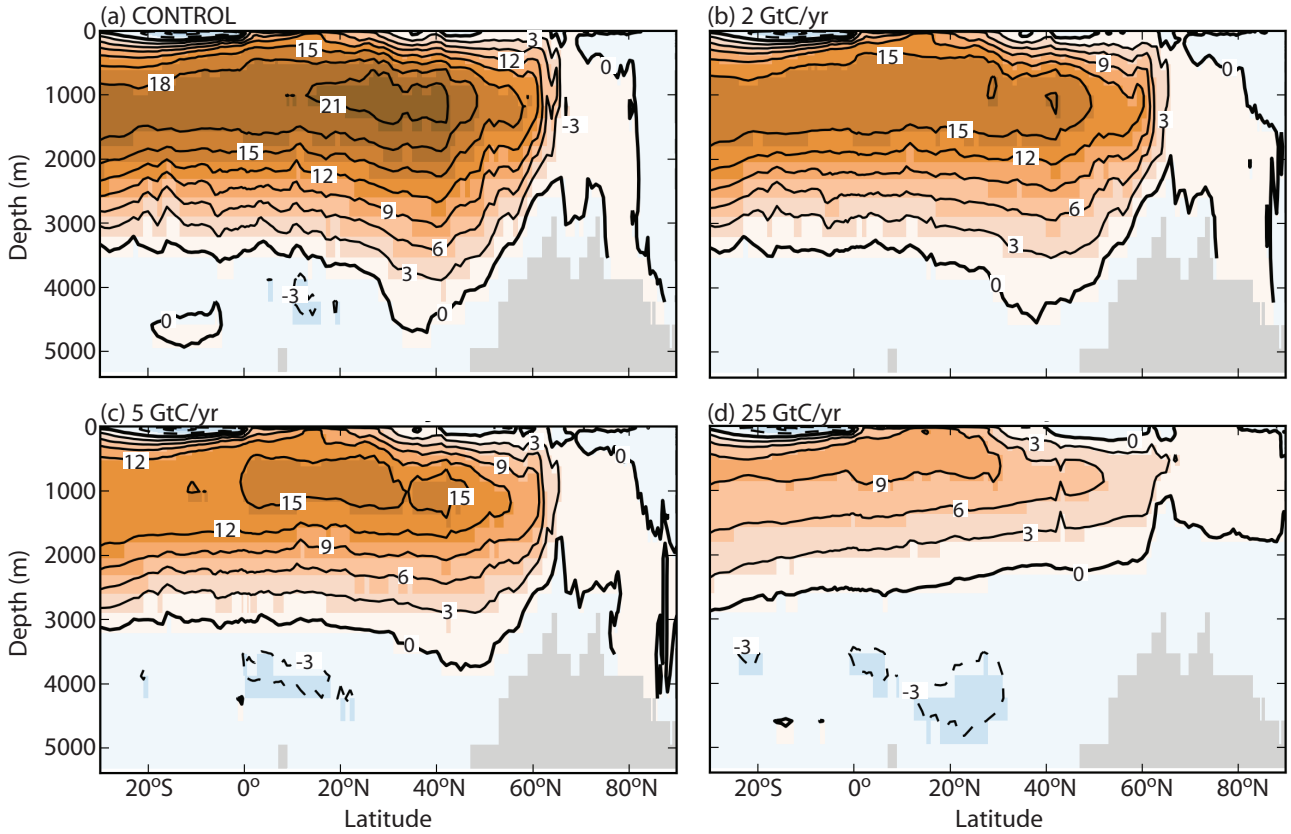
(a) CONTROL
(b) 2 GtC/yr
(c) 5 GtC/yr
(d) 25 GtC/yr
Depth (m)
0
1000
2000
3000
4000
5000
20°S
0°
20°N
40°N
60°N
80°N
Latitude

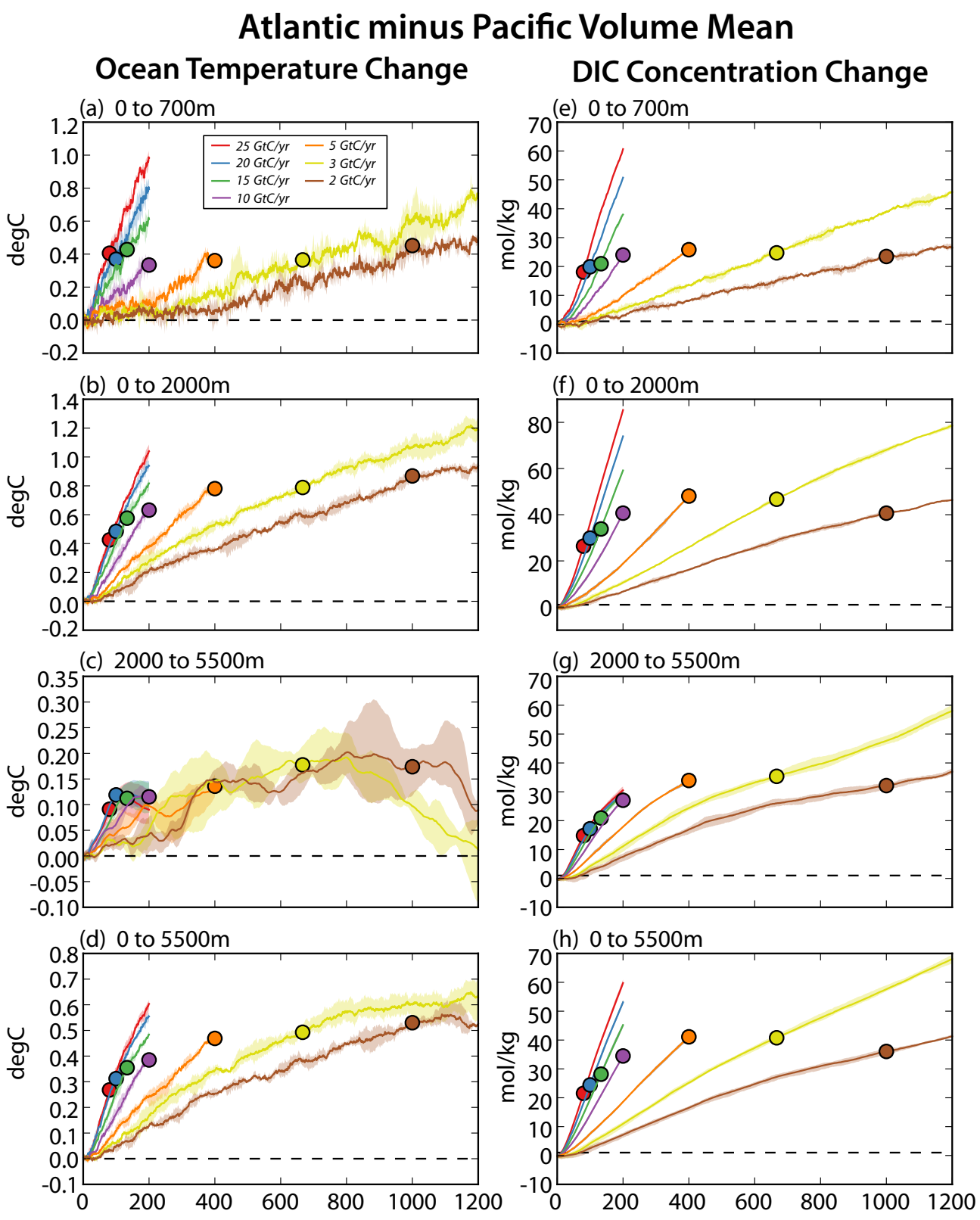
Atlantic minus Pacific Volume Mean
Ocean Temperature Change
DIC Concentration Change
(a) 0 to 700m
(b) 0 to 2000m
(c) 2000 to 5500m
(d) 0 to 5500m
(e) 0 to 700m
(f) 0 to 2000m
(g) 2000 to 5500m
(h) 0 to 5500m
25 GtC/yr
20 GtC/yr
15 GtC/yr
10 GtC/yr
5 GtC/yr
3 GtC/yr
2 GtC/yr
degC
mol/kg

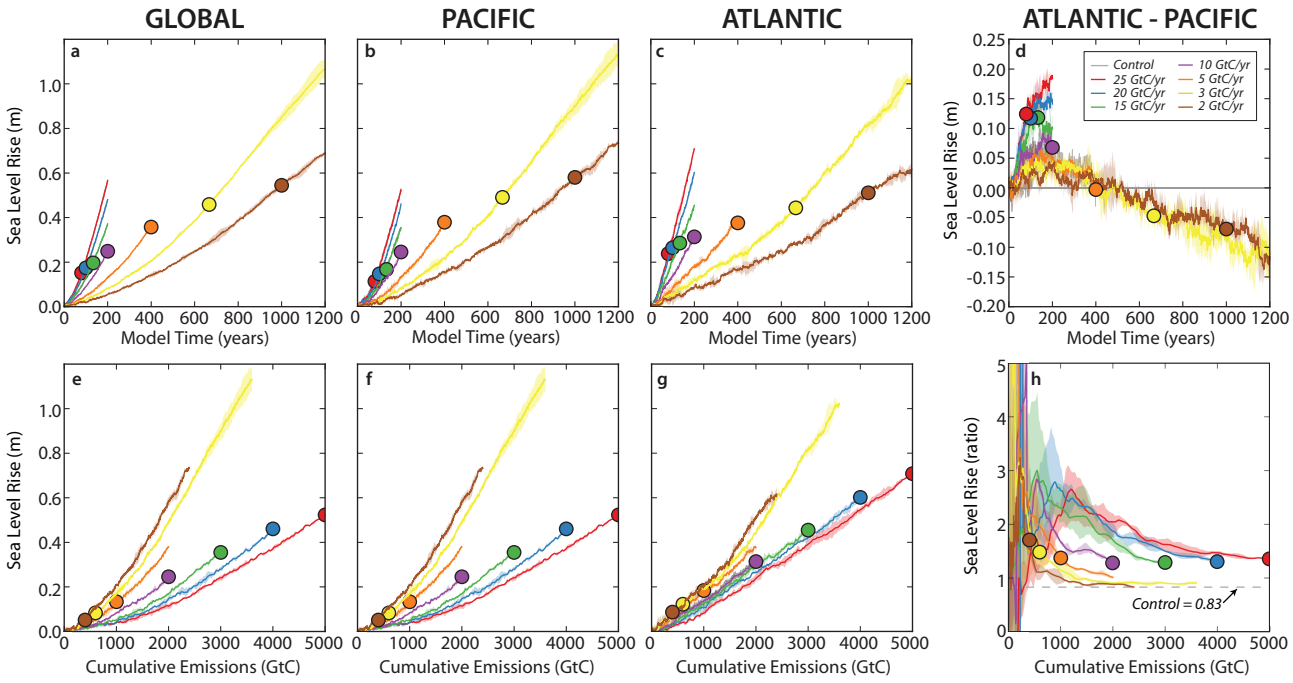
GLOBAL
PACIFIC
ATLANTIC
ATLANTIC - PACIFIC
a
b
c
d
e
f
g
h
Sea Level Rise (m)
Model Time (years)
Cumulative Emissions (GtC)
Sea Level Rise (ratio)
Control
25 GtC/yr
20 GtC/yr
15 GtC/yr
10 GtC/yr
5 GtC/yr
3 GtC/yr
2 GtC/yr
Control = 0.83

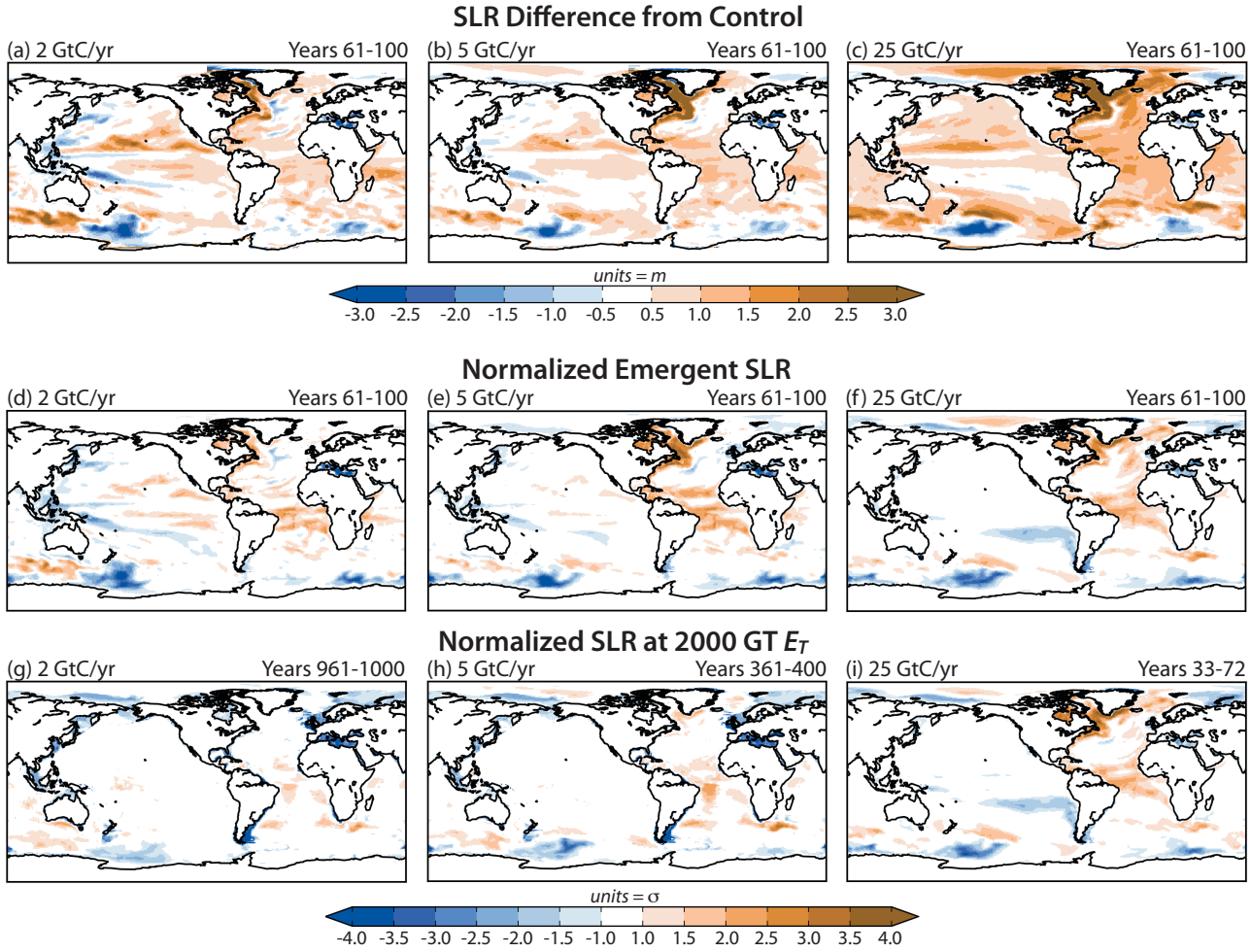
SLR Difference from Control
(a) 2 GtC/yr
Years 61-100
(b) 5 GtC/yr
Years 61-100
(c) 25 GtC/yr
Years 61-100
units = m
-3.0 -2.5 -2.0 -1.5 -1.0 -0.5 0.5 1.0 1.5 2.0 2.5 3.0
Normalized Emergent SLR
(d) 2 GtC/yr
Years 61-100
(e) 5 GtC/yr
Years 61-100
(f) 25 GtC/yr
Years 61-100
Normalized SLR at 2000 GT E_T
(g) 2 GtC/yr
Years 961-1000
(h) 5 GtC/yr
Years 361-400
(i) 25 GtC/yr
Years 33-72
units = σ
-4.0 -3.5 -3.0 -2.5 -2.0 -1.5 -1.0 1.0 1.5 2.0 2.5 3.0 3.5 4.0

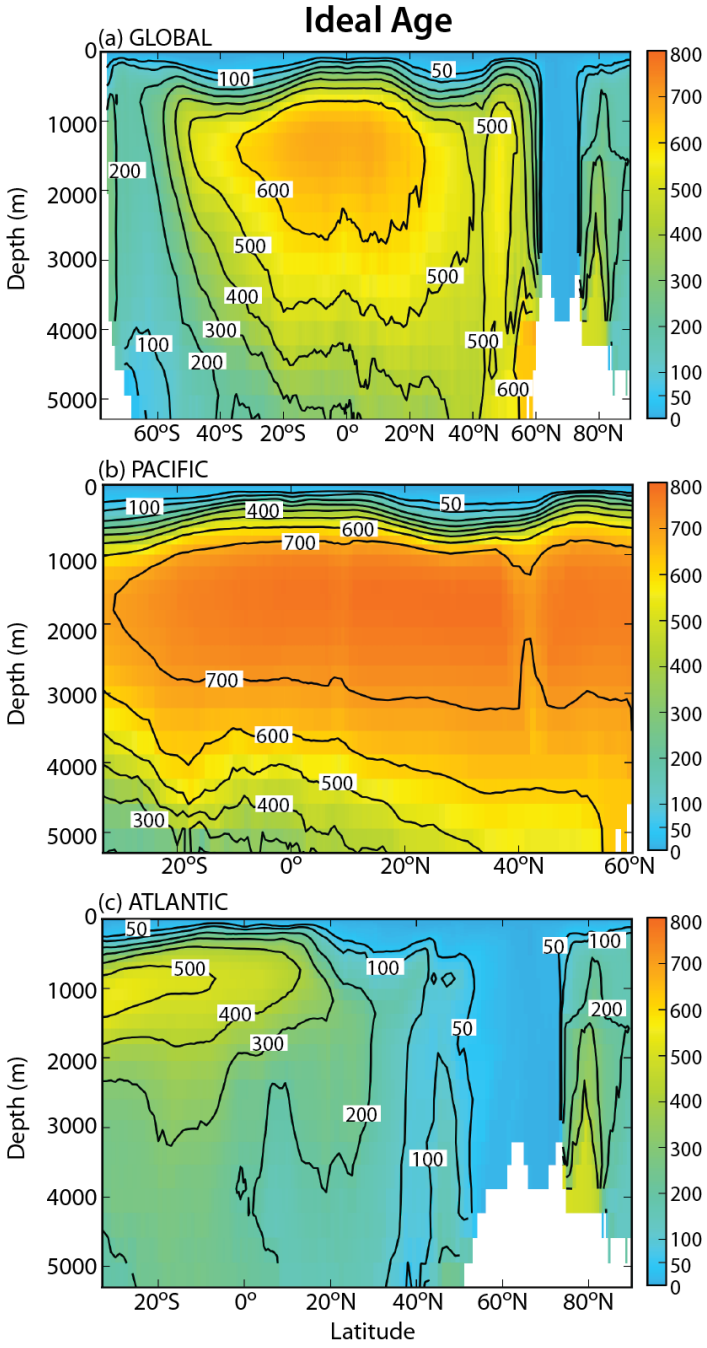

Supplementary Figure S1: Zonal average distributions of the ideal age tracer averaged over years 1 to 20 from the preindustrial control simulation. Units are years. **a**, global ocean average age (430 years). **b**, Pacific basin average age (598 years); **c**, Atlantic basin average age (226 years). Age distributions in GFDL-ESM2G are comparable with tracer observations. e.g.:

Stuvier, M., Quay, P. D. Ostlund, H. G. Abyssal water Carbon-14 distribution and the age of the world oceans. *Science* **219**, 849851 (1983).

Matsumoto, K. Radiocarbon-based circulation age of the world oceans. *J. Geophys. Res.-Oceans* **112** (2007). C09004.

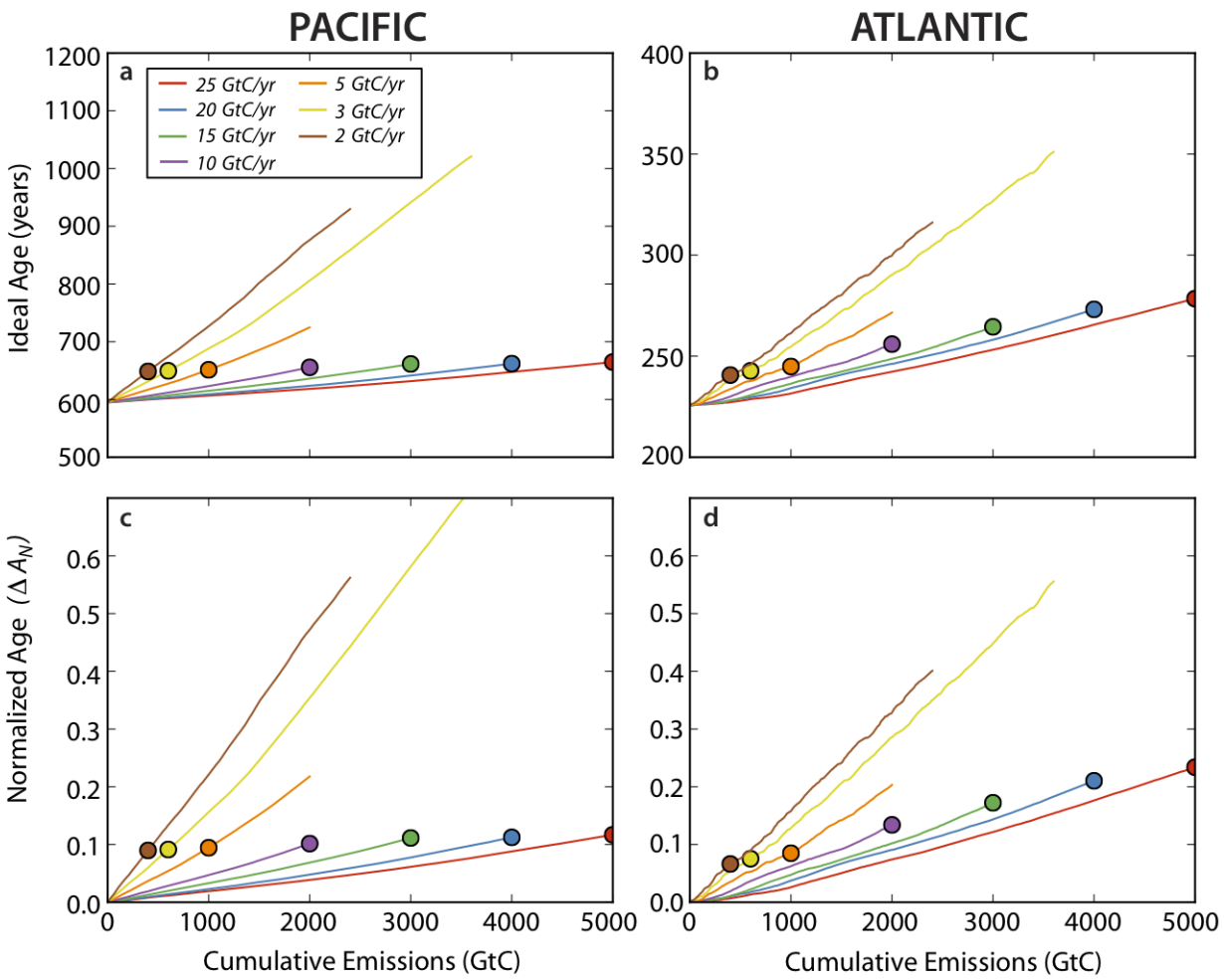

Supplementary Figure S2: Basin-average change in ideal age vs. cumulative emissions.

Units are years. Ages are plotted for the first ensemble member of each scenario. The dots represent points when the simulations reach 200 model years. **a**, Pacific basin average age vs. cumulative emissions. **b**, Atlantic basin average age vs. cumulative emissions. **c-d**, same as a-b except that the ages have been normalized by the basin-average values from the preindustrial control run (see Supplementary Figure S1, and main text).

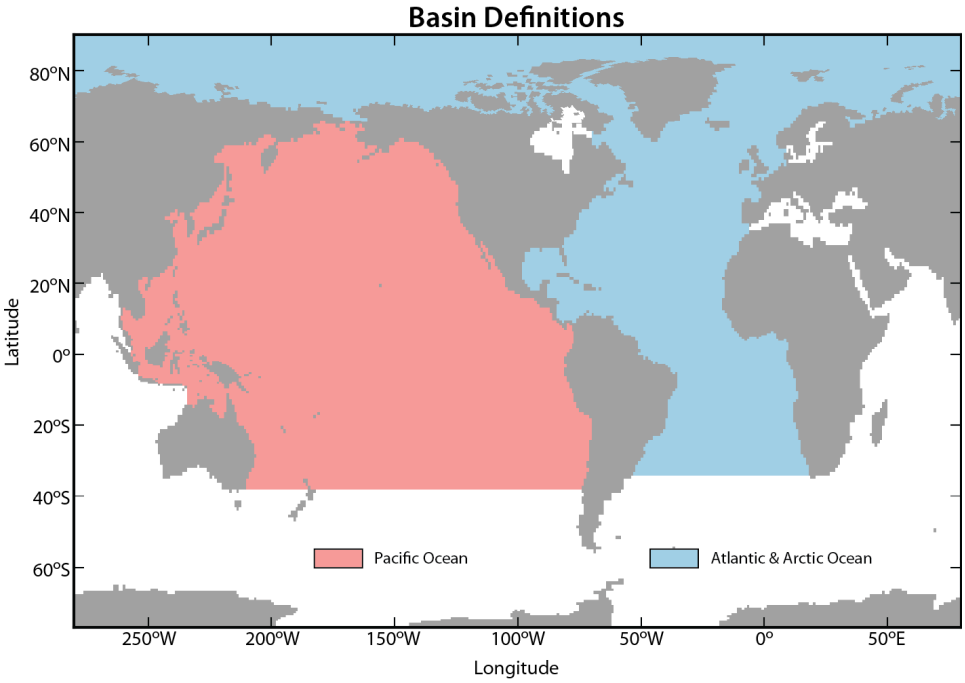

Supplementary Figure S3: Map of basins used in this study.

The Atlantic basin (blue shading) was defined as all water north of the Cape of Good Hope, South Africa and includes the Arctic Ocean but does not include Hudson Bay or the Mediterranean, Baltic, or Black Seas. The Pacific basin (coral shading) was defined as all water north of Melbourne, Australia but does not include the Indian Ocean basin.